coatings

MDPI

Article

Synergistic Effect of Elliptic Textures and H-DLC Coatings for Enhancing the Tribological Performance of CuAl10Fe5Ni5 Valve Plate Surfaces

Mengjiao Wang [1,2], Mingbo Zhu [2], Xinzheng Hu [2], Kun Liu [1,*], Xuefeng Fan [3], Xiangkai Meng [2], Xudong Peng [2] and Jinqing Wang [4]

[1] School of Mechanical Engineering, Hefei University of Technology, Hefei 230000, China; mjwangzj@163.com
[2] College of Mechanical Engineering, Zhejiang University of Technology, Hangzhou 310023, China; 15194491576@163.com (M.Z.); m15173200602@163.com (X.H.); mengxk@zjut.edu.cn (X.M.); xdpeng@126.com (X.P.)
[3] Zhejiang Changsheng Slide Bearing Co., Ltd., Jiaxing 314100, China; fxf09@tsinghua.org.cn
[4] State Key Laboratory of Solid Lubrication, Lanzhou Institute of Chemical Physics, Chinese Academy of Sciences, Lanzhou 730000, China; jqwang@licp.cas.cn
* Correspondence: liukun@hfut.edu.cn

Abstract: Axial piston pumps with compact structures and high efficiency are widely used in construction machinery. The efficiency and lifetime strongly depend on the tribological performance of the pump's valve plate pair. To enhance the tribological performance of the valve plate pair, surface textures, and H-DLC coatings were fabricated to modify the CuAl10Fe5Ni5 surfaces. The influences of elliptic textures of different sizes and textured H-DLC coatings on the surface friction and wear properties of the valve plate surface under oil lubrication were evaluated using a ring-on-disk tribometer. The results reveal that the friction and wear properties of the CuAl10Fe5Ni5 surfaces are significantly enhanced by elliptic textures, and the friction coefficient and wear rate of textured CuAl10Fe5Ni5 with E90 are maximally decreased by 95% and 87%, respectively. Compared with the surface textures and H-DLC coatings, the textured H-DLC coating has the greatest ability to reduce wear and adhesion. The wear rate of the textured H-DLC coating is further reduced by 98%. This improvement can be explained by the synergistic effect of the elliptic textures and H-DLC coatings, which are attributed to the reduced contact area, debris capture, and secondary lubrication of the elliptic textures, and increased surface hardness.

Keywords: valve plate pair; surface textures; H-DLC coatings; tribological performance; synergistic effect

Citation: Wang, M.; Zhu, M.; Hu, X.; Liu, K.; Fan, X.; Meng, X.; Peng, X.; Wang, J. Synergistic Effect of Elliptic Textures and H-DLC Coatings for Enhancing the Tribological Performance of CuAl10Fe5Ni5 Valve Plate Surfaces. *Coatings* **2024**, *14*, 1161. https://doi.org/10.3390/coatings14091161

Academic Editor: Csaba Balázsi

Received: 1 August 2024
Revised: 30 August 2024
Accepted: 6 September 2024
Published: 9 September 2024

1. Introduction

Axial piston pumps are power components that supply fluid power for hydraulic systems and have been widely applied in aerospace, marine, and construction machinery [1,2]. Axial piston pumps usually work under harsh conditions, placing further demands on them for better tribological performance. The valve plate pair is composed of a cylinder block, and the valve plate is the crucial friction pair with the largest contact area inside the piston pump, significantly affecting the pump outlet pressure and working efficiency [3]. Under fluid pulsation, the cylinder block is prone to overturning and direct contact with the valve plate, resulting in severe abrasive wear and adhesive wear, which severely reduces the piston pump outlet pressure and service life [4]. Therefore, extensive efforts have been made to improve the tribological performance of friction pairs in axial piston pumps, such as textures [5] and coatings [6].

Surface texturing has been recognized as an effective surface treatment method for enhancing the tribological properties of materials [7,8]. Zhang et al. [9] aimed to reduce the cylinder tilt behavior; a laser surface texturing (LST) technique was applied to the

steel valve plate, which is in contact with a brass cylinder. The surface texture is found to increase efficiencies by reducing wear and the cylinder tilt angle. Chen et al. [10] prepared a V-shaped texture on a soft brass surface and reported that the wear marks of the textured sample were shallower and narrower than those on the smooth surface. Zhang et al. [11] studied the tribological properties of three kinds of circular textures with different diameters of 350 μm, 500 μm, and 700 μm on the surface of a hydraulic motor shoe pair and reported that stress concentration occurred when the texture diameter was too large, resulting in an increase in the wear rate with increasing texture diameter. Research has shown that elliptical textures can significantly improve the tribological properties of material surfaces [12,13]. Babu et al. [14] demonstrated a remarkable improvement in the frictional performance of elliptical textures in combination with experimental and numerical studies compared with untextured. The results revealed a maximum friction reduction of 87% with elliptical textures compared with the untextured substrate. The surface texture improves the tribological properties but is generally damaged or even completely worn off due to wear after a certain period of friction where the surface graphics are weakened until they disappear. Research has shown that surface coating modification is an effective solution to this issue [15,16]. The surface coating has excellent tribological properties, which provides an effective approach for improving the lubrication and wear resistance of valve plate pairs [17,18]. Zhao et al. [19] improved the friction and wear resistance of an EHA pump valve plate by preparing a TiAlN coating on the surface and grounding a tin bronze cylinder block. Compared with those of the samples subjected to the nitriding treatment, the friction coefficient and wear rate of the valve plate surface after the TiAlN coating treatment were reduced by 52.55%~64.9% and 12%~14%, respectively. Owing to their special chemical and physical properties, such as high hardness, high chemical inertia, low friction, and high wear resistance, diamond-like carbon coatings (DLCs) are widely used as lubricating and wear-resistant protective coatings [20]. There are various types of DLC coatings on the market, but the most popular and effective ones used for tribological applications are hydrogenated amorphous carbon H-DLC and hydrogen-free tetrahedral amorphous carbon DLC coatings. H-DLC coatings (hardness in the range of 15–50 GPa) consist of an amorphous structure composed of strongly bonded random carbon–carbon and carbon–hydrogen networks with mainly sp^2 (graphitic-like) and sp^3 (diamond-like) type bonding. H-free DLC coatings (hardness in the range of 30–80 GPa) have a hydrogen-free random carbon–carbon network that is mostly sp^3 hybridized. Above all, H-free DLCs have some advantages over H-DLC, namely, higher hardness, a lower friction coefficient in humid air, and higher thermal stability [21]. Liu et al. [22] studied the superlubricity of hydrogenated diamond-like carbon (H-DLC) film in a vacuum was achieved against four different friction pairs (ZrO_2, Al_2O_3, Si_3N_4, and SiC) due to the formation of graphene and nanoscrolls in transfer layer as well as the graphitization of contacted substrate. Liu et al. [23] studied the effects of a normal load and contact pair on the tribological performance of DLC coatings. The results show that the friction coefficient and wear rate of the DLC coating surface decrease with increasing load and that the degree of wear of the DLC coating increases with increasing friction pair hardness (DLC film against ZrO_2, bearing steel, and SiC balls). The TEM and Raman characterization results further indicated that the key factor for the low friction of DLC coatings is the degree of graphitization of the transfer layer, rather than the continuity and density of the transfer layer. Owing to the problems that the surface texture is easily filled by wear debris and the lubrication failure of coatings after shear under harsh working conditions, combining the surface texture and coating is an effective method to improve the tribological performance of friction pairs due to the synergistic effect [24–27]. Xing et al. [28] studied the tribological properties of Si_3N_4/TiC ceramic surfaces via a combination of DLC hard coatings and microtextures and reported that the lubrication of the DLC coating and debris capture of the texture had a good synergistic effect and that the textured DLC coating surfaces were beneficial for decreasing friction, adhesion, and wear. He et al. [29] reported the tribological behaviors of textured DLC films with microdimple densities of 39%, 52%, and 58% and compared them with those of the

untextured DLC films. The results showed that the textured DLC coating with a density of 52% had the lowest average friction coefficient and wear rate due to the friction-induced graphitization of the textured layer and entrapment of wear debris in the microdimples. Based on the above reviews, a combination of DLC coatings and surface textures results in excellent tribological properties. However, few studies have focused on the combination of texture density and surface morphology with DLC coatings to improve friction and wear properties. The synergistic effect of DLC coatings and surface textures with different sizes under oil lubrication has not been investigated, and the reinforcement mechanism is still not clear.

In this study, laser elliptical textures and H-DLC coatings were produced on CuAl10Fe5Ni5 valve plate surfaces. The motivation of this work is to investigate the effects of laser elliptical textures with different sizes and synergistic tribological properties of elliptical textures combined with H-DLC coatings on the surface of a CuAl10Fe5Ni5 valve plate. Friction and wear tests were performed using a ring-on-disk universal friction tester under oil lubrication conditions. The effects of the texture size and textured H-DLC coatings, and the relevant friction and wear mechanisms under oil lubrication conditions were illustrated in detail.

2. Experiment Details

2.1. Laser Surface Texturing and Coating Deposition

The CuAl10Fe5Ni5 and GCr15 specimens used in the experiments were purchased from Jiashan Jingcheng Machinery Co., Ltd. The chemical compositions are listed in Table 1. Prior to laser texturing, the surfaces of the CuAl10Fe5Ni5 specimens were sequentially polished with 400#, 800#, 1200#, 1500#, and 2000# SiC sandpapers to achieve surface roughness *R*a values less than 0.05 μm, and then all specimens were ultrasonically cleaned for 15 min with acetone and anhydrous ethanol solutions. The CuAl10Fe5Ni5 specimens were subsequently subjected to laser microtexture processing with different size parameters using a YLP-20f laser marking machine (Shenzhen, China). The design of the laser surface texturing parameters is shown in Figure 1. The laser experimental parameters were set as follows: the laser power was 8 W, the scanning speed was 200 mm/s, the pulse repetition frequency was 25 kHz, the fill spacing was 8 μm, and the scanning times were 5 times. Elliptical textures with long axes of 85 μm, 127 μm, 170 μm, and 212 μm and depths of 25–30 μm, with a surface density of 5%, were prepared in ring areas with inner and outer radii of 11 mm and 15 mm, respectively. The textures with different size parameters were denoted as E60, E90, E120, and E150. After laser texturing, the textured CuAl10Fe5Ni5 specimens were further ground with 2000# SiC sandpaper and polished with W0.5 diamond polishing liquid to remove the recast layer at the texture surface edges. Finally, the specimens were ultrasonically cleaned in anhydrous ethanol for 20 min and then dried. The optical microscope, three-dimensional morphologies, and two-dimensional profiles of the textured specimens were characterized by a 3D confocal laser microscope (Olympus-OLS-5000, Japan). A physical vapor deposition method was used to apply an H-DLC coating on both the CuAl10Fe5Ni5 substrate and the textured CuAl10Fe5Ni5 surface. The arc ion plating process begins with high-energy arc discharge to generate a plasma of evaporated metal sources. H-DLC coating was deposited on polished CuAl10Fe5Ni5 structure and textured CuAl10Fe5Ni5 specimens. Firstly, after the gas is pumped to a pressure lower than 1×10^{-3} Pa, Ar is injected at a 16 cm^3/min rate. The Cr transition layer is deposited for 5 min under target current 3.0 A and bias voltage −70 V. Then the graphite target current is set to 3.5 A, and the flow rate of reaction gas isobutane is 16 cm^3/min. H-DLC coating was deposited for 4 h. This gave rise to two types of samples: substrate + coating (S+D) and textured DLC coating (S+T+D).

Table 1. Chemical compositions of the CuAl10Fe5Ni5 samples.

Elements	Cu	Al	Fe	Ni	Mn
Content/wt%	Balance	8.0–11.0	3.4–5.5	3.4–6.5	≤3.0

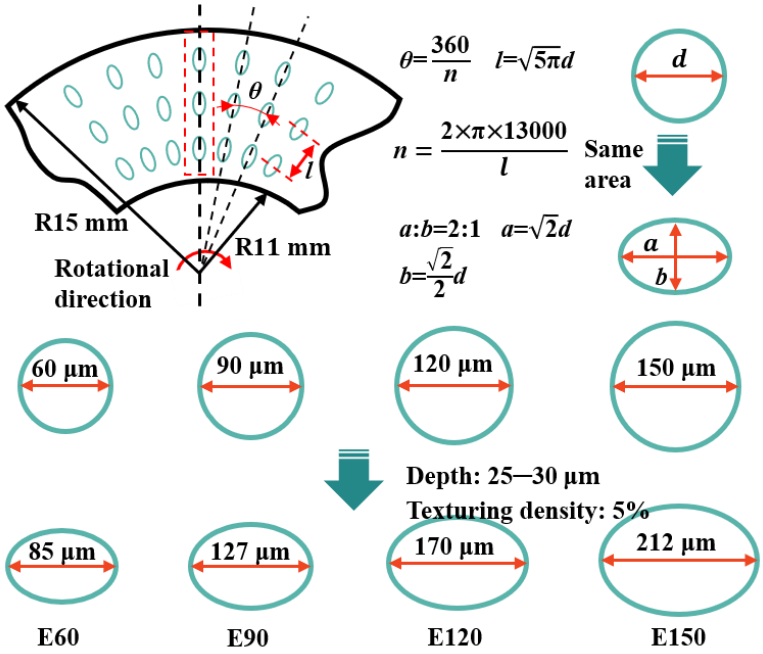

Figure 1. Diagram of texture parameter design.

2.2. Friction and Wear Tests

Figure 2 shows a schematic diagram of the friction and wear tests. Rotary sliding friction tests were performed using a ring-on-disk MMU-12 tribometer (Jinan, China) to evaluate the friction and wear performance of the elliptical textures and H-DLC coatings. The friction test equipment and schematic diagram are shown in Figure 2. The upper specimen was a GCr15 ring with dimensions of Φ22 mm × 30 mm × 14 mm unidirectional rotating with the spindle, and the lower specimen was a fixed CuAl10Fe5Ni5 component with dimensions of 37 mm × 37 mm × 12 mm. Four kinds of lower specimens with different elliptical texture sizes were used for friction tests: E60, E90, E120, and E150, respectively (as shown in Figure 1); the texture density was 5%. Subsequently, four different lower specimens were used for friction tests: smooth substrate surface (S), E90-textured substrate surface (S+T), smooth surface with H-DLC coatings (S+D), and E90-textured surface with H-DLC coatings (S+T+D). All the friction tests were performed with the normal load of 1634 N (contact pressure is 5 MPa) and a rotation speed of 300 r/min at room temperature. The rotation direction was parallel to the short-axis direction of the elliptical texture. Each test duration was 30 min and repeated at least 3 times to eliminate random test errors. During friction tests, the lower specimen was completely immersed in L-HM-46 anti-wear hydraulic oil. The real-time friction coefficient curves were obtained by collecting the friction torque of the lower specimens, and the friction temperature curves were obtained by measuring the oil temperature with a temperature sensor.

After the friction tests, the two-dimensional profiles of wear tracks were measured by a 3D confocal laser microscope (Olympus-OLS-5000, Japan). The worn morphologies and element distributions on the worn surfaces of the CuAl10Fe5Ni5 and GCr15 specimens were observed by scanning electron microscopy (∑IGMA, Germany) and detected by an EDS spectrometer (Bruker Nano XFlash Detector 5010, Germany).

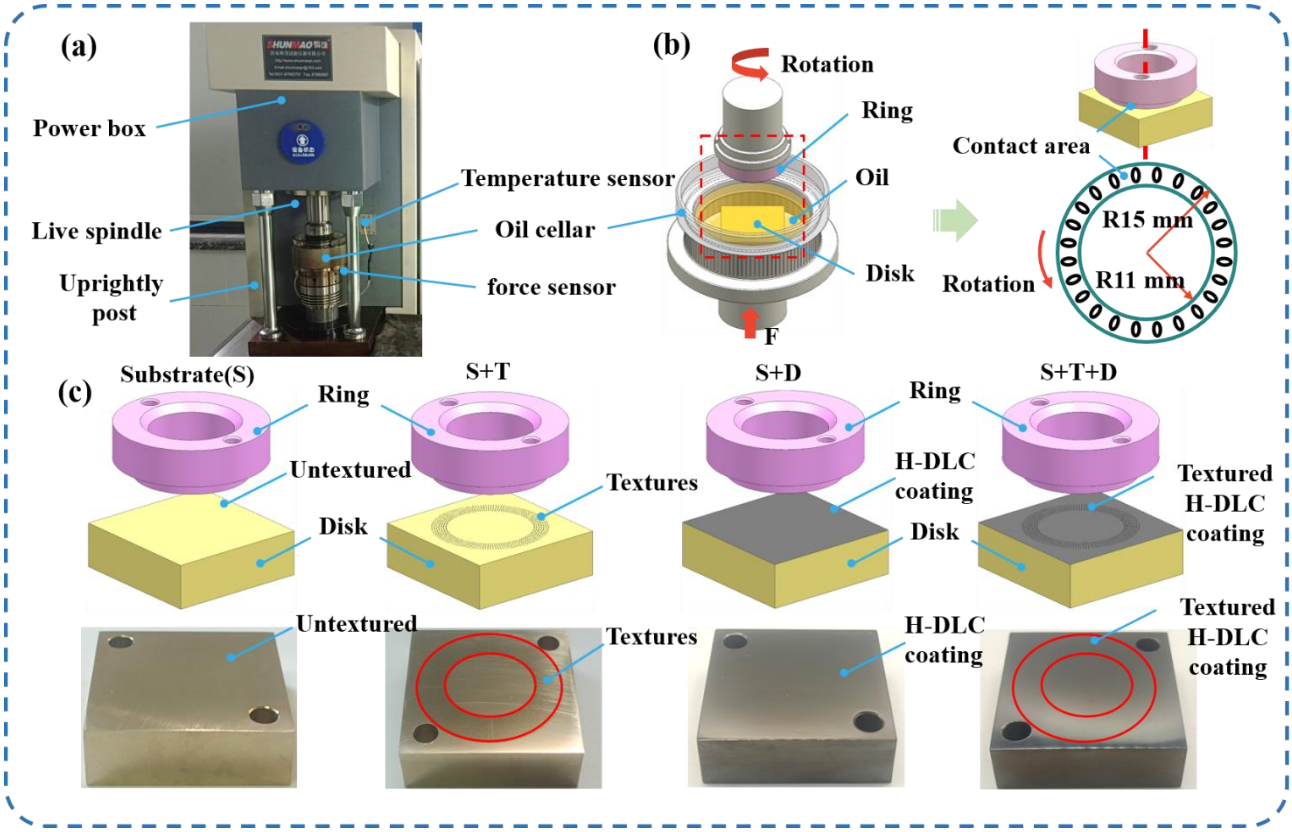

Figure 2. (**a**) MMU-12 ring-on-disk tribometer; (**b**) schematic diagram of the friction and wear tests; and (**c**) sample naming.

3. Results and Discussion

3.1. Characterization of Morphology and Structure

Figure 3 shows the three-dimensional morphologies and two-dimensional cross-sectional profiles of the substrate and textured CuAl10Fe5Ni5. Figure 3(a1–e1) display microscopy images of the substrate and textured CuAl10Fe5Ni5 with elliptical textures of E60, E90, E120, and E150, respectively. Figure 3(b2–e2) present the corresponding three-dimensional morphologies of elliptical textures of different sizes, whereas Figure 3(b3–e3) show the corresponding two-dimensional cross-sectional profiles of these surfaces. Figure 3(b3–e3) show that the depth of the elliptical textures is 25–30 μm, and uneven phenomena occur at the bottom of the texture grooves. As the texture size increases, this phenomenon becomes more pronounced, primarily because of the thermal effects of laser processing. The surface of the CuAl10Fe5Ni5 material undergoes vaporization, and a large amount of CuAl10Fe5Ni5 is ejected from the molten pool to form a texture. Some material that is not fully ejected resolidifies at the bottom of the texture grooves after cooling, leading to a phenomenon of recasting and resulting in an uneven morphology at the base of the texture [30].

Surface roughness is an important parameter affecting the tribological characteristics during the running-in stage. Relevant studies have shown that a relatively high initial roughness can shorten the running-in period. Nevertheless, roughness that is too high will result in a relatively high surface wear rate of the material [31]. Figure 4 shows the surface roughness of the substrate and the textured CuAl10Fe5Ni5 surfaces. Surface roughness measurements were taken along the radial direction of the contact area of the upper and lower samples, with specific attention given to the long axes of different-sized elliptical textures. As shown in Figure 4, the surface roughness of the textured CuAl10Fe5Ni5 is significantly greater than that of the smooth substrate owing to the presence of micrometer-sized pits on the textured sample surface, and the surface roughness first increases and then decreases with increasing elliptical texture size. For E90, the surface roughness is greater

than that for the other sizes. In Figure 4, all the surface roughness parameters represent the height parameters, and the size of the roughness is the result of the synthesis of the texture edge bulge and the texture groove bottom roughness. With increasing in texture size, the inhomogeneity of the bottom of the texture groove increases, but the number of textures in the selected area decreases (Figure 3(b2–e2)), so the surface roughness first increases and then decreases with increasing texture size.

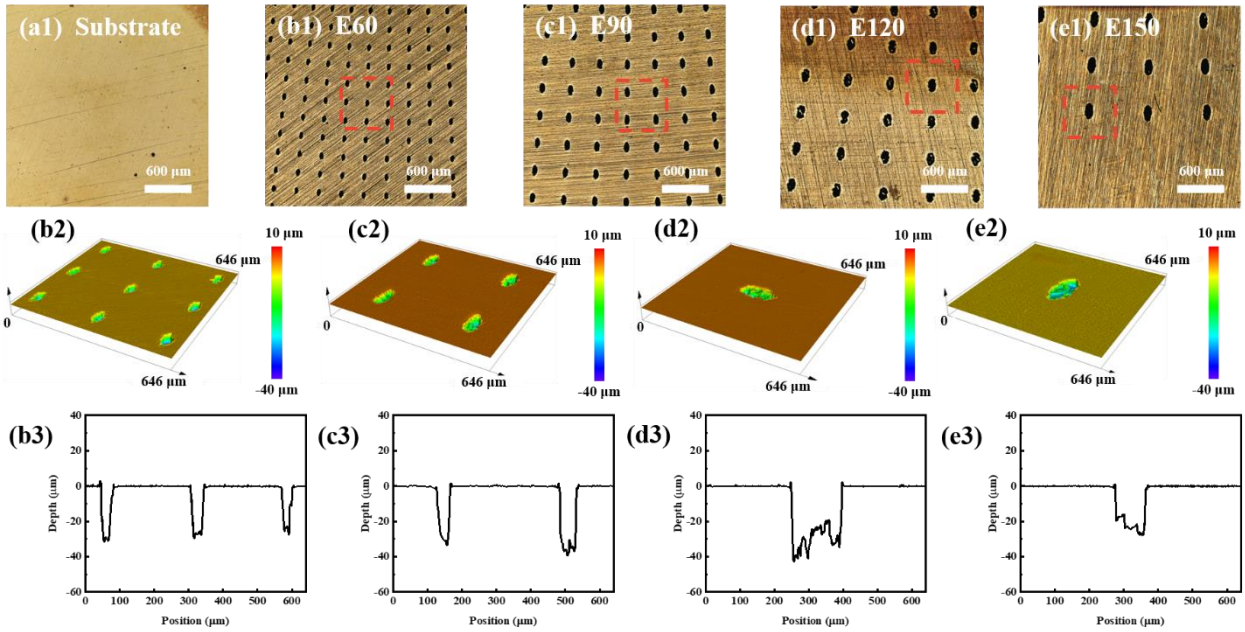

Figure 3. Surface morphologies of (**a1**) CuAl10Fe5Ni5 substrate and textured surfaces with different dimensions of (**b1**–**b3**) E60; (**c1**–**c3**) E90; (**d1**–**d3**) E120; and (**e1**–**e3**) E150.

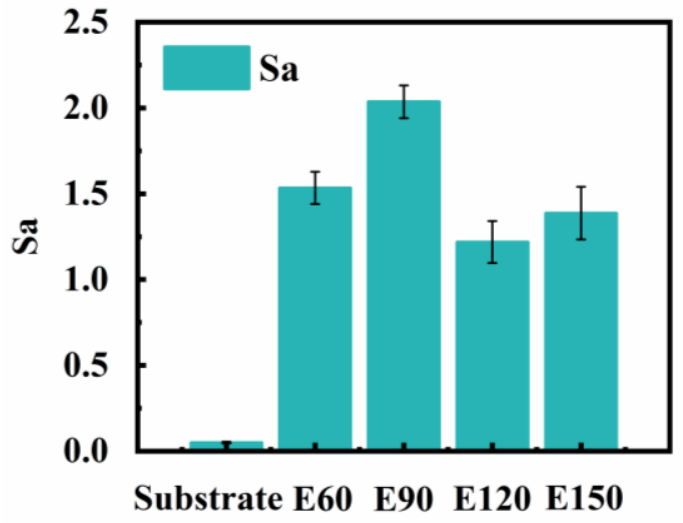

Figure 4. Surface roughness of the substrate and textured CuAl10Fe5Ni5 specimens.

3.2. Tribological Properties of Textured CuAl10Fe5Ni5 Surfaces

Figure 5a,b show the friction coefficient curves and average friction coefficients of the substrate and textured CuAl10Fe5Ni5 specimens, respectively. Figure 5a shows that the friction coefficient between the textured CuAl10Fe5Ni5 and GCr15 initially increased but then remained relatively stable during the friction process. With increasing time, all the friction coefficients tend to increase, and after the run-in period, the friction coefficients tend to stabilize. The friction coefficients of all textured specimens were smaller than those

of the smooth substrate specimens after a short run-in period. With increasing elliptical texture size, the friction coefficient first decreases but then increases, and the fluctuation range of the friction coefficient curve also decreases gradually and then increases in the stable stage. The E90 elliptical texture has the smoothest and most stable friction coefficient curve. Owing to the different surface roughnesses of the elliptical textures with different sizes, the time of the run-in stage of the textured CuAl10Fe5Ni5 specimens is different. Except for the E150 elliptical texture, the run-in stage of the textured surfaces with different sizes is shorter than that of the substrate surface, because the relatively large initial surface roughness of the textured surface is conducive to shortening the run-in period. When the texture size is too large (E150), the friction coefficient curve fluctuates sharply, and there is no obvious stable stage because the negative influence of the texture increases the surface friction resistance, resulting in severe wear on the textured CuAl10Fe5Ni5 surface. Figure 5b shows that the average friction coefficient of the textured surface is smaller than that of the smooth substrate surface under oil lubrication conditions. The average friction coefficient is 6%–95% lower than that of smooth substrates. The decreased friction coefficient of the textured specimens might be attributed to the elliptical textures playing the dual roles of wear debris and lubricating oil reservoirs. With increasing texture size, the friction coefficient decreases with increasing texture ability to store wear debris and lubricating oil. When the texture size increases to E90, the lubrication and storage wear debris advantages of the textured surface are more obvious, and the friction coefficient is 95% lower than that of the smooth substrate surface. With increasing texture size, the stress concentration at the texture edge increases, and the friction coefficient increases gradually under the influence of the stress concentration at the texture edge. When the texture size is increased to E150, the friction coefficient approaches that of the substrate because of the stress concentration at the texture edge, and the advantage of the texture storing lubricating oil and wear debris is that it cannot have an excellent anti-friction effect. Figure 5c,d show the surface friction temperature curve and average temperature rise of textured CuAl10Fe5Ni5. According to Figure 5d, the average temperature rise of the textured surface is smaller than that of the substrate surface, which corresponds to the change of the average friction coefficient in Figure 5b, indicating that relatively less friction heat is generated by the textured surface. In addition, during the rotation of the upper GCr15 specimen, the pits on the textured surface have a larger contact area with the lubricating medium, which has a better heat transfer effect than the CuAl10Fe5Ni5 substrate does, which is conducive to strengthening the convective heat transfer effect and reducing the temperature rise of the end face [32–34], especially in the case of the optimal texture size E90. The temperature rise of the E90-textured surface is 92% lower than that of the substrate surface.

Figure 6 presents the wear rates and two-dimensional cross-sectional profiles of the wear scars of the substrate and textured CuAl10Fe5Ni5 specimens. As shown in Figure 6a, except for the E150 elliptical texture specimens, the wear rates of the textured CuAl10Fe5Ni5 are all lower than those of the substrate, indicating a superior wear resistance. The E90 elliptical texture has the significantly lowest wear rate, which is 87% lower than that of the smooth substrate surface. In addition, the two-dimensional cross-sectional profile in Figure 6d shows that the wear scars of the E90 elliptical texture surface are flat and that the wear is relatively slight because the elliptical plays the dual role of wear debris and lubricating oil reservoirs [35–37]. When the texture size is too small (E60), the storage lubrication medium effect of the texture is limited, and the wear is greater than the E90. If the texture size is too large (E150), the texture surface is negatively affected by stress concentration, resulting in increased wear, resulting in a higher wear rate than that of the substrate surface, and the corresponding wear depth is significantly greater than that of the substrate surface.

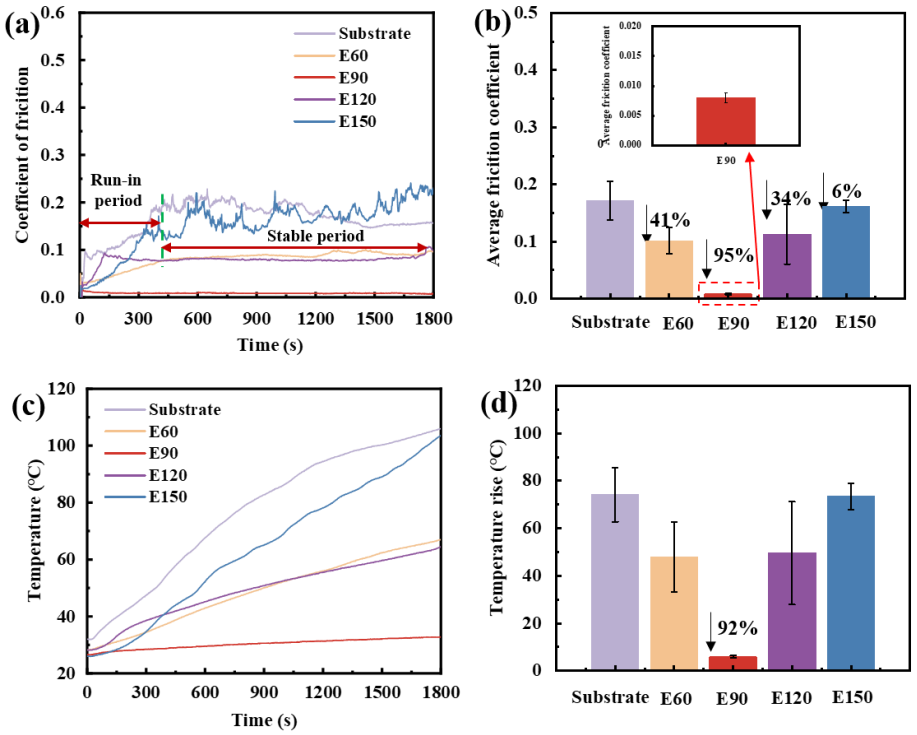

Figure 5. (**a**) Friction coefficient curve; (**b**) average friction coefficient; (**c**) temperature curve; and (**d**) average temperature rise of the substrate and textured CuAl10Fe5Ni5 samples.

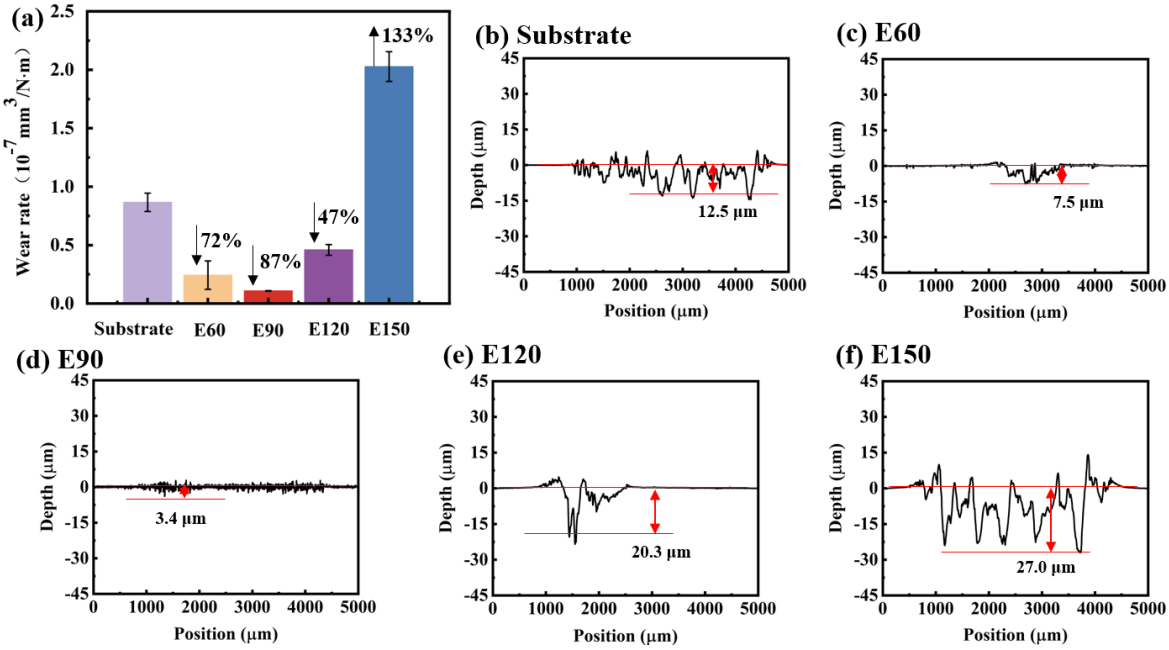

Figure 6. Wear performance of the substrate and textured CuAl10Fe5Ni5: (**a**) wear rate and (**b**–**f**) two-dimensional cross-sectional profile.

Figure 7 shows SEM micrographs of the worn surfaces of the substrate, textured CuAl10Fe5Ni5, and GCr15. As shown in Figure 7a, severe wear with adhesions and plows is produced on the wear scars of the CuAl10Fe5Ni5 substrate surface, owing to the influence of microcutting caused by the hard microconvex surfaces of GCr15. Compared with those on the substrate surface, the wear scars on the textured surface are reduced and milder, and shallow plows without obvious adhesions are found, resulting in abrasive wear. In

the case of an appropriate texture size E90, the surface wear of CuAl10Fe5Ni5 is relatively slight, and only slight abrasive wear occurs, which is due to storing and supplementing the lubricating medium for the friction interface under the action of loading, exerting secondary lubrication, and then achieving significantly lower wear. For the specimens with E60, E120, and E150 elliptical textures, the texture of the worn surface is partially worn out and loses its storage ability, resulting in relatively severe surface wear. The storage effect of excessively small texture size (E60) is limited, whereas the impact of stress concentration is limited. When the texture size is excessively large (E150), the decreased contact area increases the average contact stress on the sliding surface and thus increases wear on the surface [38]. Figure 7(a3–e3) show the worn morphologies of the GCr15 upper specimens. Furrowing and adhesion are the main phenomena on the worn surface. When the texture size is E90, the surface wear of GCr15 is relatively slight with no obvious plows or adhesions on the wear scars, and slight abrasive wear occurs.

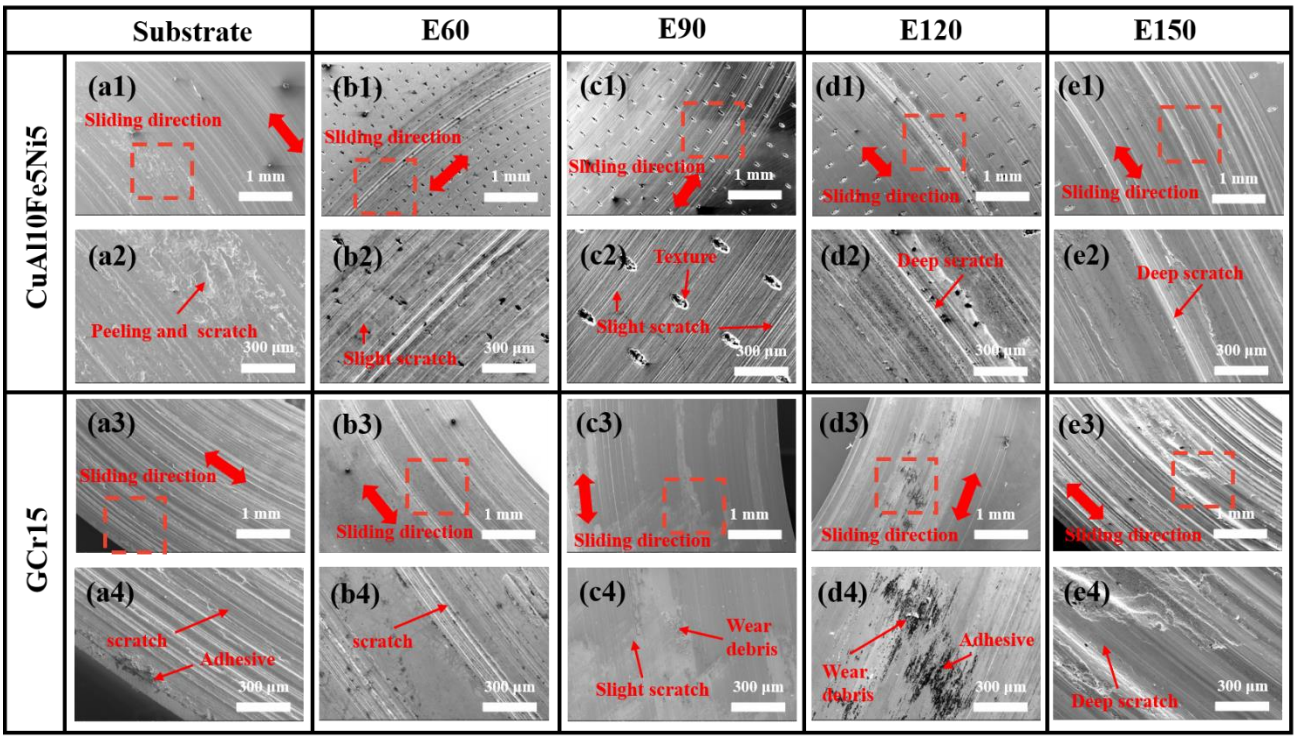

Figure 7. SEM images of the substrate and textured CuAl10Fe5Ni5 surfaces after wear: (**a1**–**a4**) substrate; (**b1**–**b4**) E60; (**c1**–**c4**) E90; (**d1**–**d4**) E120; and (**e1**–**e4**) E150.

To further investigate the worn morphology and mechanism, SEM and EDS mapping of GCr15 counterfaces sliding against the substrate and E90-textured CuAl10Fe5Ni5 specimens were carried out, as shown in Figure 8. As shown in Figure 8a, after the upper specimen GCr15 slides against the CuAl10Fe5Ni5 substrate, the surface of GCr15 is severely worn, and there are many plows on the worn surface. The corresponding EDS mapping shows that the worn surface is full of O and Cu. These results indicate that the CuAl10Fe5Ni5 substrate is transferred to the surface of GCr15, resulting in adhesive wear and oxidative wear. When GCr15 slid against the E90 elliptical texture surface, the ploughing of the worn surface of GCr15 significantly decreased. According to the EDS spectra, few O and Cu elements can be observed on the worn surface, indicating that E90 elliptical textures are the most effective in reducing adhesion wear, abrasive wear, and oxidation wear of the upper GCr15 specimen under oil lubrication conditions.

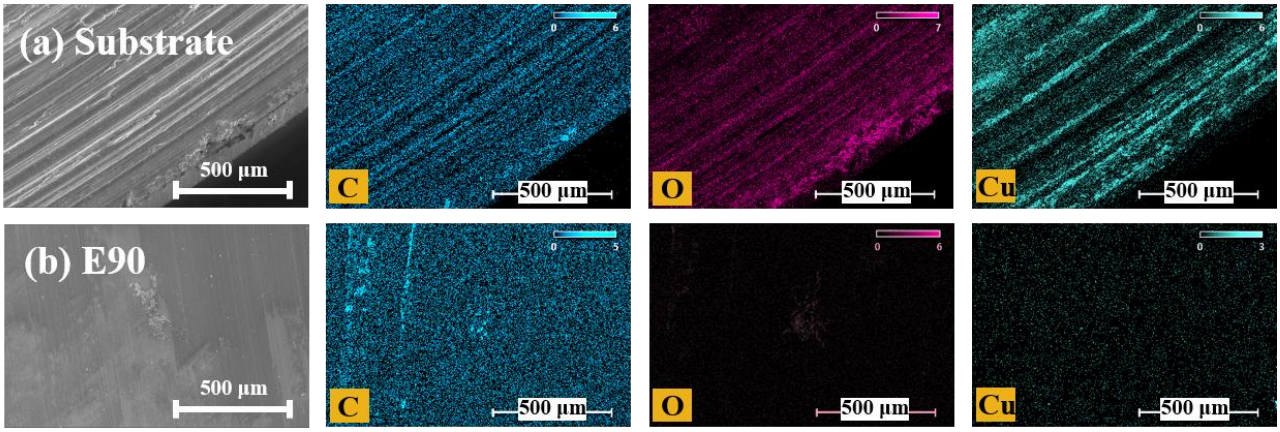

Figure 8. SEM images and EDS maps of GCr15 counterfaces sliding against the substrate and E90-textured CuAl10Fe5Ni5.

3.3. Tribological Properties of Textured H-DLC Coatings

To further improve the tribological properties of the CuAl10Fe5Ni5 surface, H-DLC coatings were deposited on the CuAl10Fe5Ni5 substrate (S+D) and the E90 elliptical texture surface (S+T+D). The friction coefficient and friction temperature are shown in Figure 9. In Figure 9a, the friction coefficient of the CuAl10Fe5Ni5 substrate is relatively high and fluctuates greatly during the friction process, and the average friction coefficient is ~0.17. Compared with the substrate, the E90 elliptical texture and H-DLC coating are beneficial to stabilize and reduce the friction coefficient because of the wear debris capture and lubricant storage of the texture, as well as the good lubrication characteristics of the H-DLC coatings. The friction coefficient is reduced by 95% and 94%, indicating an excellent anti-friction effect. The friction coefficient of the textured H-DLC coating surface (S+T+D) is ~0.08, greater than that of the textured (S+T) and coated (S+D) surfaces. However, the scraping of the edges increases the friction coefficient of the textured coating. Figure 9c,d show the friction temperature curves and average temperature rise of the substrate, E90 elliptical texture, H-DLC coating, and textured H-DLC coating. The H-DLC coating significantly reduces the friction temperature rise of the CuAl10Fe5Ni5 substrate. Moreover, the trends of the friction temperatures and average temperature increases of the CuAl10Fe5Ni5 substrate, S+T, S+D, and S+T+D specimens corresponded to the friction coefficients and average friction coefficients shown in Figure 9a,b.

Figure 10 shows the wear rates of the CuAl10Fe5Ni5 substrate, E90 elliptical texture, H-DLC coating, and textured H-DLC coating. Compared with those of the substrate, the wear rates of the elliptical textures and H-DLC coatings significantly decreased, and the wear rates decreased by 87% and 91%, respectively. The texture functions to store wear particles and lubricating oil for secondary lubrication. Compared with the CuAl10Fe5Ni5 substrate, the H-DLC coating has greater hardness and excellent lubrication properties. The high hardness and self-lubrication of the H-DLC coating significantly improved the wear resistance of the CuAl10Fe5Ni5 surface. In addition, the wear rate of the textured H-DLC coating (S+T+D) is further reduced to 1.88×10^{-9} $mm^3/(N \cdot m)$, which is lower than that of both the E90 elliptical texture (S+T) and the H-DLC coating (S+D). The elliptical texture can provide storage space for the lubricating medium required for oil lubrication at the friction interface, and the lubricating oil can be added to the friction interface during the friction process. It plays a role in secondary lubrication, and the coating and lubricating oil form solid–liquid composite lubrication under oil lubrication, further reducing the wear rate of the textured H-DLC coating [28].

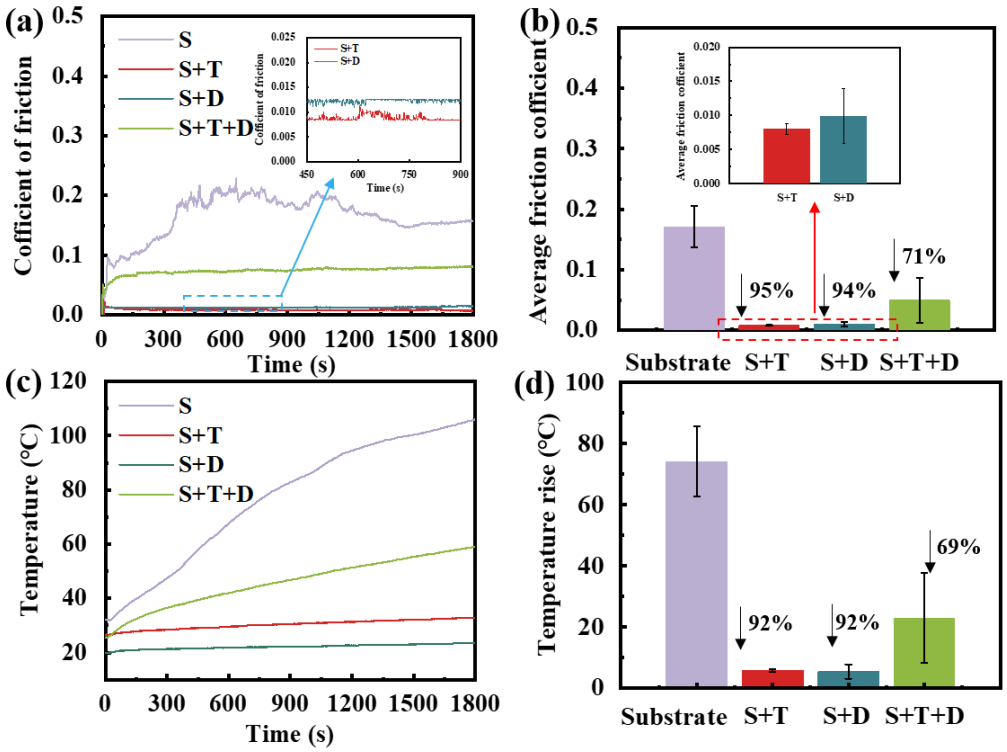

Figure 9. The friction coefficients and friction temperatures of the CuAl10Fe5Ni5 surfaces deposited with the H-DLC coatings are as follows: (**a**) friction coefficient curve; (**b**) average coefficient of friction; (**c**) temperature curve; and (**d**) average temperature increase.

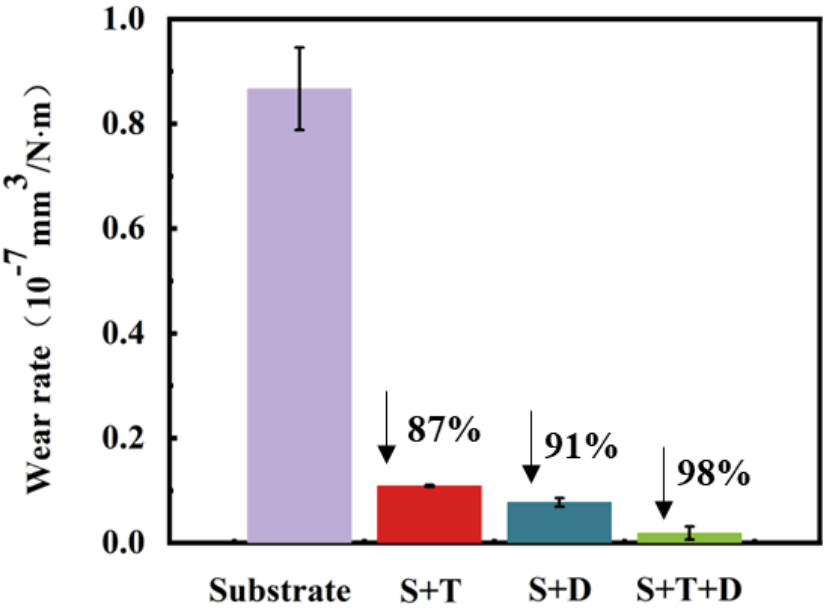

Figure 10. Wear rate of the CuAl10Fe5Ni5 substrate, E90 elliptical texture, H-DLC coating, and textured H-DLC coating.

Figure 11 shows the SEM morphology of the H-DLC coating, textured H-DLC coating on CuAl10Fe5Ni5, and counterfaces of GCr15. As a result, the wear scar is narrow, and a series of plows along the rotation direction on the worn surface of S+D indicates severe abrasive wear (Figure 11(a1)) and scratches on the corresponding upper GCr15 worn surface (Figure 11(c1)). Compared with the substrate, the lubricating coating with low shear strength at the contact interface led to a significant reduction in adhesions and

abrasive wear (Figure 7a). Figure 11(a1,b1) shows that after the textured H-DLC coating is deposited on the surface of CuAl10Fe5Ni5, the surface contact area of the friction pair is reduced by the texture, and the adverse influence of stress concentration easily occurs on the texture edge, resulting in the surface wear scars of the textured coating (S+T+D) being significantly greater than those of the H-DLC coating (S+D). However, the texture of the H-DLC film might be attributed to the dual functions of capture of wear debris and oil storage during the friction process, the wear scar is shallower than that on S+D. According to the analysis in Figure 11(c1,d1), compared with the H-DLC coating, the textured H-DLC coating reduces the abrasive wear caused by the secondary entry of abrasive chips into the wear interface due to the chip-absorbing effect of the texture, resulting in only a few scratches on the surface of the textured H-DLC coating and slight abrasive wear on the GCr15 surface.

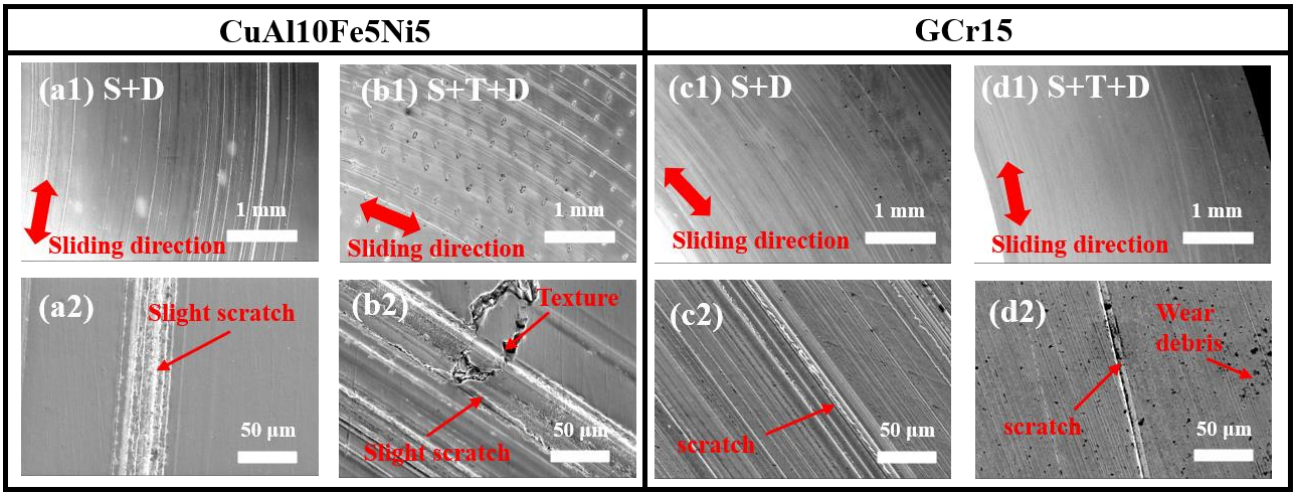

Figure 11. SEM images of the morphology of the CuAl10Fe5Ni5 surface deposited with the H-DLC coating and the GCr15 surface. (**a1**,**a2**) S+D of the CuAl10Fe5Ni5; (**b1**,**b2**) S+T+D of the CuAl10Fe5Ni5; (**c1**,**c2**) S+D of the GCr15; (**d1**,**d2**) S+T+D of the GCr15.

The optimal-sized elliptical texture facilitates the capture of wear particles and stores lubricating oil on the surface texture, reducing the friction and wear of GCr15 and CuAl10Fe5Ni5 surfaces. The existence of surface texture increases the contact area between the CuAl10Fe5Ni5 and lubricating oil, which effectively reduces the friction temperature rise, which is more prominent for the CuAl10Fe5Ni5 than the GCr15 substrate.

In summary, the friction mechanism is proposed and illustrated in Figure 12. The surface wear failure mode of CuAl10Fe5Ni5 is mainly dominated by abrasive wear and oxidation wear. The optimal texture size is determined as E90. On the one hand, the microtexture collects abrasive particles and impurities generated during the whole sliding process, which inhibits severe abrasive wear [39]. On the other hand, microtexturing offers secondary lubrication, which acts as an oil storage site [40]. Under deformation and shear, the lubricating fluid in the microtexture enters and lubricates the friction interface, which significantly improves the lubrication state of the friction couple. The surface texture not only decreases the friction coefficient but also reduces the friction temperature increase, inhibiting Cu transfer on the surface of GCr15. Owing to the high hardness and self-lubrication of the H-DLC coating, the CuAl10Fe5Ni5 surface only suffers slight abrasive wear. In addition, the textured H-DLC coating surface is beneficial to the storage effect of the texture, which collects wear debris of the H-DLC coating and further reduces the wear rate of the material.

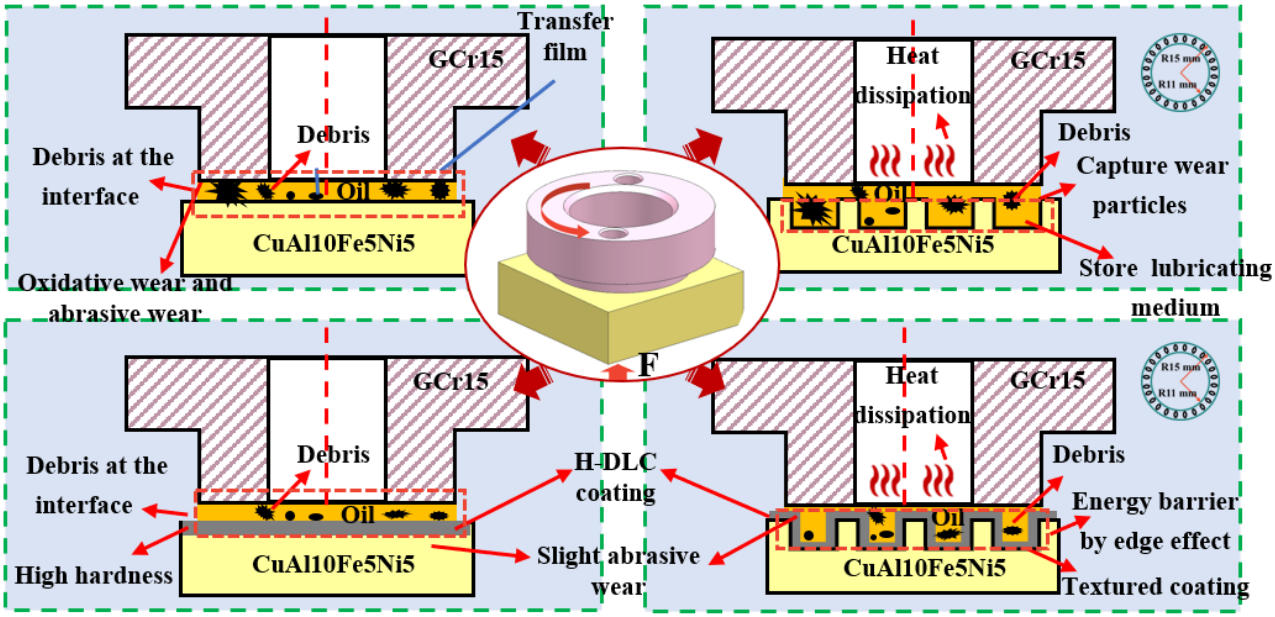

Figure 12. Schematic diagram of the friction and wear mechanism of the textured H-DLC coating on the CuAl10Fe5Ni5 surface.

4. Conclusions

In this work, laser elliptical textures of different sizes were fabricated on CuAl10Fe5Ni5, and H-DLC coatings were subsequently deposited on the textured surface. The friction and wear behaviors of the textured H-DLC coating CuAl10Fe5Ni5 coupled with the GCr15 counterpart were investigated by sliding friction tests under oil lubrication. The influences of texture size and coating modification on the friction and wear properties of the valve plate surface under oil lubrication were studied, and the main conclusions are as follows:

(1) Under the appropriate size design, the elliptical texture has better lubrication and anti-wear effects on the CuAl10Fe5Ni5 surface. After textured as E90, the friction coefficient is reduced by 95%, and the wear rate is reduced to 1.09×10^{-8} mm^3/(N·m).

(2) Elliptic textures of different sizes play a role in storing wear debris and lubricating media, but their anti-friction effect is affected by changes in texture size and surface roughness. The friction and wear properties of the CuAl10Fe5Ni5 surface can be further improved by incorporating a textured H-DLC coating surface with an appropriate texture size.

(3) Different degrees of abrasive wear occurred on the substrate surface, the textured CuAl10Fe5Ni5 surface, the substrate + H-DLC coating surface, and the textured H-DLC coating surface. After grinding with the substrate surface, slight oxidation and adhesive wear occurred on the surface of GCr15. The introduction of texture improved the adhesion resistance of the surface of the friction pair, and only slight abrasive wear occurred on the surface.

In addition, the surface texture may also possess thermal, optical, or even electronic properties to be discovered.

Author Contributions: Conceptualization, M.W.; methodology, M.W., M.Z. and X.H.; formal analysis, M.Z. and X.H.; investigation, M.W., M.Z. and X.H.; data curation, M.Z. and X.H.; writing—original draft preparation, M.W.; writing—review and editing, K.L., X.M., X.P. and J.W.; project administration, X.F.; funding acquisition, M.W. and X.M. All authors have read and agreed to the published version of the manuscript.

Funding: This work is financially supported by the Natural Science Foundation of Zhejiang Province (Grant No. LQ22E050020), the National Natural Science Foundation of China (Grant No. 52105217), the Open Project of the State Key Laboratory of Solid Lubrication, Lanzhou Institute of Chemical Physics, Chinese Academy of Sciences (Grant No. LSL-2109), and the State Key Program of the National Natural Science Foundation of China (Grant No. U2241246).

Institutional Review Board Statement: Not applicable.

Informed Consent Statement: Not applicable.

Data Availability Statement: All data generated or analyzed during this study are included in this article.

Conflicts of Interest: Author Xuefeng Fan was employed by the company Zhejiang Changsheng Slide Bearing Co., Ltd. The remaining authors declare that the research was conducted in the absence of any commercial or financial relationships that could be construed as a potential conflict of interest.

References

1. Suo, X.; Jiang, Y.; Wang, W. Hydraulic axial plunger pump: Gaseous and vaporous cavitation characteristics and optimization method. *Eng. Appl. Comp. Fluid.* **2021**, *15*, 712–726. [CrossRef]
2. Wang, Q.; Wang, H.; Yuan, S.; Wang, J.; Lin, N.; Liu, Z.; Wu, Y. Research progress on service damage and protection of axial piston pump sliding shoe pair. *Surf. Technol.* **2023**, *6*, 126–139.
3. Xu, L. *Study on the Lubrication Characterisics of the Valve Plate Bearing in Hydraulic Axial Piston Pump*; Beijing Institute of Technology: Beijing, China, 2016.
4. Wang, H.; Lin, N.; Yuan, S.; Liu, Z.; Yu, Y.; Zeng, Q.; Wu, Y. Structural improvement, material selection and surface treatment for improved tribological performance of friction pairs in axial piston pumps: A review. *Tribol. Int.* **2024**, *198*, 109838. [CrossRef]
5. Chen, Y.; Zhang, J.; Xu, B.; Chao, Q.; Liu, G. Multi-objective optimization of micronscale surface textures for the cylinder/valve plate interface in axial piston pumps. *Tribol. Int.* **2019**, *138*, 316–329. [CrossRef]
6. Kalin, M.; Majdic, F.; Vižintin, J.; Pezdirnik, J.; Velkavrh, I. Analyses of the long-term performance and tribological behavior of an axial piston pump using diamondlike-carbon-coated piston shoes and biodegradable oil. *J. Tribol-T ASME* **2008**, *130*, 011013-1-8. [CrossRef]
7. Yuan, S.; Lin, N.; Wang, W.; Zhang, H.; Liu, Z.; Wu, Y. Correlation between surface textural parameter and tribological behaviour of four metal materials with laser surface texturing (LST). *Appl. Surf. Sci.* **2022**, *583*, 152410. [CrossRef]
8. Wang, H.; Tian, L.; Zheng, J.; Yang, D.; Zhang, Z. The synergetic effects of laser texturing and super-hydrophobic coatings on improving wear properties of steel. *Tribol. Int.* **2022**, *173*, 107657. [CrossRef]
9. Zhang, J.; Chen, Y.; Xu, B.; Chao, Q.; Zhu, Y.; Huang, X. Effect of surface texture on wear reduction of the tilting cylinder and the valve plate for a high-speed electro-hydrostatic actuator pump. *Wear* **2018**, *414*, 68–78. [CrossRef]
10. Chen, L.; Liu, Z.; Song, W. Process-surface morphology-tribological property relationships for H62 brass employing various manufacturing approaches. *Tribol. Int.* **2020**, *148*, 106320. [CrossRef]
11. Zhang, D.; Li, Z.; Wang, L.; Kong, L.; Gao, F.; Wang, Q. Study on tribological properties of boronized and textured composite surface and its application on camshaft connecting-rod type hydraulic motor. *Wear* **2021**, *482*, 203964. [CrossRef]
12. Xu, Y.; Zheng, Q.; Abuflaha, R.; Olson, D.; Furlong, O.; You, T.; Tysoe, W.T. Influence of dimple shape on tribofilm formation and tribological properties of textured surfaces under full and starved lubrication. *Tribol. Int.* **2019**, *136*, 267–275. [CrossRef]
13. Wang, H.; Li, Y.; Zhu, H. Influence of geometrical parameters and arrangement Mode of elliptic cylindrical Texture on lubrication and antifriction performance. *J. Tribol.* **2016**, *36*, 77–83. [CrossRef]
14. Babu, P.V.; Ismail, S.; Ben, B.S. Experimental and numerical studies of positive texture effect on friction reduction of sliding contact under mixed lubrication. *P. I. Mech. Eng. J—J. Eng.* **2021**, *235*, 360–375. [CrossRef]
15. Chen, P.; Xin, X.; Shao, T.; La, Y.; Li, J. Effect of triangular texture on the tribological performance of die steel with TiN coatings under lubricated sliding condition. *Appl. Surf. Sci.* **2016**, *389*, 361–368. [CrossRef]
16. Xin, T.; Pei, H.; Shucai, Y. Coating and micro-texture techniques for cutting tools. *J. Mater. Sci.* **2022**, *57*, 17052–17104. [CrossRef]
17. Evaristo, M.; Fernandes, F.; Cavaleiro, A. Influence of the alloying elements on the tribological performance of DLC coatings in different sliding conditions. *Wear* **2023**, *526*, 204880. [CrossRef]
18. Zhuo, X.; Cao, J.; Huang, H.; Liu, L.; Suo, X.; Ye, P.; Abbas, Z. Cavitation erosion resistance and tribological performance of PAI/PI/EP soft coating on 20CrMo. *Wear* **2024**, *536*, 205176. [CrossRef]
19. Zhao, J.; Fu, Y.; Wang, M.; Fu, J.; Chao, Q.; Wang, S.; Deng, M. Experimental research on tribological characteristics of TiAlN coated valve plate in electro-hydrostatic actuator pumps. *Tribol. Int.* **2021**, *155*, 106782. [CrossRef]
20. Wang, S.; Zhang, G.; Fu, A.; Cao, X.; Yin, C.; Liu, Z. Investigation of the tribological properties and corrosion resistance of multilayer Si-DLC films on the inner surfaces of N80 steel pipes. *Coatings* **2024**, *14*, 385. [CrossRef]
21. Leonardo, I.; Farfan, C.; Julio, A.; Seungjoo, L.; Merve, U.; Ali, E. Tribological behavior of H-DLC and H-free DLC coatings on bearing materials under the influence of DC electric current discharges. *Wear* **2023**, *522*, 204709.
22. Liu, Y.; Jiang, Y.; Sun, J.; Wang, L.; Liu, Y.; Chen, L.; Qian, L. Durable superlubricity of hydrogenated diamond-like carbon film against different friction pairs depending on their interfacial interaction. *Appl. Surf. Sci.* **2021**, *560*, 150023. [CrossRef]
23. Liu, Y.; Wang, L.; Liu, T.; Zhang, P. Effect of normal loads and mating pairs on the tribological properties of diamond-like carbon film. *Wear* **2021**, *486*, 204083. [CrossRef]

24. Arslan, A.; Masjuki, H.H.; Varman, M.; Kalam, M.A.; Quazi, M.M.; Al Mahmud, K.A.H.; Habibullah, M. Effects of texture diameter and depth on the tribological performance of DLC coating under lubricated sliding condition. *Appl. Surf. Sci.* **2015**, *356*, 1135–1149. [CrossRef]
25. Vallinot, I.B.; de la Guerra Ochoa, E.; Otero, J.E.; Tanarro, E.C.; Martínez, I.F.; Varela, J.A.S. Individual and combined effects of introducing DLC coating and textured surfaces in lubricated contacts. *Tribol. Int.* **2020**, *151*, 106440. [CrossRef]
26. Xing, Y.; Zhu, M.; Wu, Z.; Li, Z.; Bai, S.; Zhang, K.; Liu, L. High-temperature tribological properties of Si3N4/TiC ceramic with bionic surface textures and DLC coatings. *Tribol. Int.* **2023**, *186*, 108648. [CrossRef]
27. Qi, H.; Hu, C.; Zhang, G.; Yu, J.; Zhang, Y.; He, H. Comparative study of tribological properties of carbon fibers and aramid particles reinforced polyimide composites under dry and sea water lubricated conditions. *Wear* **2019**, *436*, 203001. [CrossRef]
28. Xing, Y.; Wang, X.; Du, Z.; Zhu, Z.; Wu, Z.; Liu, L. Synergistic effect of surface textures and DLC coatings for enhancing friction and wear performances of Si_3N_4/TiC ceramic. *Ceram. Int.* **2022**, *48*, 514–524. [CrossRef]
29. He, D.; He, C.; Li, W.; Shang, L.; Wang, L.; Zhang, G. Tribological behaviors of in-situ textured DLC films under dry and lubricated conditions. *Appl. Surf. Sci.* **2020**, *525*, 146581. [CrossRef]
30. Xing, Y.; Luo, C.; Wan, Y.; Huang, P.; Wu, Z.; Zhang, K. Formation of bionic surface textures composed by micro-channels using nanosecond laser on Si_3N_4-based ceramics. *Ceram. Int.* **2021**, *47*, 12768–12779. [CrossRef]
31. Jiao, W.; Xia, Y.; Ma, H.; Zhu, Z.; Xia, S. Effect of running-in on the low-pressure tribological performance of valve plate pair in axial piston pumps. *Wear* **2023**, *532*, 205113. [CrossRef]
32. Lou, D.; Yang, D.; Dong, C.; Chen, C.; Jiang, H.; Li, Q.; Liu, D. Enhancement of pool boiling heat transfer by laser texture-deposition on copper surface. *Appl. Surf. Sci.* **2024**, *661*, 160015. [CrossRef]
33. Zhou, Y.; Peng, X.; ZHAO, W. Texture heat transfer mechanism and structure optimization of the outer Surface of mechanical seal moving ring. *Tribology* **2020**, *40*, 538–550.
34. Yu, M.; Peng, X.; Meng, X.; Jiang, J.; Ma, Y. Influence of cavitation on the heat transfer of high-Speed mechanical seal with textured side wall. *Lubricants* **2023**, *11*, 378. [CrossRef]
35. Kovalchenko, A.; Ajayi, O.; Erdemir, A.; Fenske, G.; Etsion, I. The effect of laser surface texturing on transitions in lubrication regimes during unidirectional sliding contact. *Tribol. Int.* **2005**, *38*, 219–225. [CrossRef]
36. Amanov, A.; Tsuboi, R.; Oe, H.; Sasaki, S. The influence of bulges produced by laser surface texturing on the sliding friction and wear behavior. *Tribol. Int.* **2013**, *60*, 216–223. [CrossRef]
37. Etsion, I. State of the art in laser surface texturing. *J. Trib.* **2005**, *127*, 248–253. [CrossRef]
38. Kumar, C.S.; Patel, S.K. Effect of WEDM surface texturing on Al_2O_3/TiCN composite ceramic tools in dry cutting of hardened steel. *Ceram. Int.* **2018**, *44*, 2510–2523. [CrossRef]
39. Zhang, Y.; Deng, J.; Meng, Y.; Yue, H. Tribological performance of steel guideway with biomimetic hexagonal micro-textures. *Surf. Eng.* **2020**, *36*, 756–764. [CrossRef]
40. Li, C.; Yang, X.; Wang, S.; Wang, Y.; Lu, C.; Cao, J. Study on friction and lubrication characteristics of surface with unidirectional convergence texture. *Coatings* **2019**, *9*, 780. [CrossRef]